ELSEVIER

Physica D 129 (1999) 93–114

PHYSICA D

# Multifractal asymptotic modeling of the probability density function of velocity increments in turbulence

J.M. Tchéou [a,b], M.E. Brachet [a,*], F. Belin [a], P. Tabeling [a], H. Willaime [a]

[a] *Laboratoire de Physique Statistique de l'École Normale Supérieure, associe au CNRS et aux Universités Paris 6 et 7, 24 Rue Lhomond, 75231 Paris Cedex 05, France*

[b] *Direction Scientifique AXA-UAP, 9 Place Vendôme, 75052 Paris Cedex 01, France*

Received 2 February 1998; received in revised form 18 November 1998; accepted 1 December 1998
Communicated by U. Frisch

**Abstract**

Moments and probability density functions (PDF) of (absolute value) velocity increments $|v(x+\ell)-v(x)|$ in turbulence are linked by simple integral relations. It is shown that the steepest descent method can be applied to evaluate the integrals if the moments (the absolute value structure functions) obey multifractal scaling laws of the type $\langle|v(x+\ell)-v(x)|^n\rangle = A_n\ell^{\zeta_n}$. A double asymptotic relation then relates the moments to the PDF. The dominant (exponential) terms of the asymptotic relation naturally yield the Legendre transform that is at the core of the Parisi–Frisch model of inertial-range intermittency. Using the asymptotic relation, the PDF can be reconstructed from the multifractal exponent spectrum $\zeta_n$ and the statistics of large scale moments. On the basis of experimental results, it is shown that moments are quantitatively represented by multifractal scaling laws and large scale Gaussian (or quasi-Gaussian) statistics. The large scale at which the statistics are Gaussian (or quasi-Gaussian) is determined from inertial-range data alone and is of the order of the integral scale for Taylor-scale Reynolds numbers $R_\lambda$ in the range (300–2200). This representation of moments together with the double asymptotic relations is able to reconstruct quantitatively the experimental inertial-range PDF. Analytic expressions (She-Lévêque and Log-normal) of scaling exponents are both shown to lead to reconstructed PDF with systematic deviations from experiment. 

*PACS:* 07.05.Kf; 47.53.+n; 47.25.−c; 05.40.+j

*Keywords:* Turbulence; Intermittency; Probability density function; Moments; Steepest descent method; Multifractal scaling law

## 1. Introduction

The existence and characterization of scaling laws in fully developed turbulence has been the object of considerable interest in the last 50 years. Perhaps the best known example is the famous prediction by Kolmogorov in 1941 (K41) [1–3] of the scaling of order-$n$ moments of velocity increments over a distance $\ell$ as $\ell^{\zeta_n}$, with $\zeta_n = n/3$ for $n = 2$

* Corresponding author.

0167-2789/99/$ – see front matter 
PII: S0167-2789(98)00307-8

and $n = 3$. This prediction was latter extrapolated to arbitrary $n$. However, the actual situation is known to be more complex than this K41 model. In 1962, Kolmogorov and Obukhov [4,5] introduced the log-normal (K62) model which is defined using a random multiplicative process that was presented as a model of the (random) fluctuating cascade of energy in turbulence. Although the K62 model is known to lead to inconsistency in incompressible turbulence in the limit of high Reynolds numbers [6], several other models using the concept of a random cascade were developed. An example is the 1964 'black and white' model of Novikov and Stewart [7]. A reformulation of the black and white model using inertial-range quantities, the so-called $\beta$-model, was proposed in 1978 by Frisch, Sulem and Nelkin [8]. Independently, at the end of the 1960s, Mandelbrot applied the notion of non-integer Hausdorff dimension (fractal dimension) to the measure of the sets where energy is dissipated [9,10]. A few years later, several experimental teams measured the exponents $\zeta_n$, for high $n$-vaues [11–13]. These experiments showed that neither the log-normal nor the $\beta$ models were adequate. In 1985, in order to interpret the experimental results, Frisch and Parisi [14] introduced the multifractal model that represents the exponents $\zeta_n$ as the Legendre transform of a function $\mu(h) = 3 - D(h)$, interpreted as the Hausdorff co-dimension of a family of sets. Let us recall that the scaling is termed 'unifractal' if the exponent $\zeta_n$ is an affine function of $n$ and 'multifractal' if it is a non-linear (convex) function of $n$. Our starting point will be the probabilistic reformulation of the multifractal model by Frisch [6], which gives for the velocity, a formulation analogous to that called 'Cramér renormalization' by Mandelbrot [15].

The main purpose of the present paper is to quantitatively reconstruct the PDF of velocity increments in turbulence from the known values of the scaling exponents $\zeta_n$. Such a reconstruction is nontrivial. Indeed, the probabilistic reformulation is known to put some constraints on the PDF but not to determine it in a unique way (see [6], p. 194, note 44). Nevertheless, reconstruction is possible because of two properties. First, the large scale moments follow Gaussian (or quasi-Gaussian statistics). Thus, it is possible to know the moments at all (inertial) scales by using both the scaling laws (with known $\zeta_n$) and the large scale statistics. Second, using multifractal scaling, it is possible to asymptotically evaluate the integrals that relate moments to PDF. The resulting asymptotic formula is used to reconstruct the PDF.

The asymptotic formula is obtained in the following way. The moments are linked to the PDF by a Mellin transform that is equivalent, after a logarithmic change of variable, to a two-sided Laplace transform. The Laplace transform can be inverted in the complex plane by a Fourier transform. Both the Laplace and the Fourier transforms can be evaluated asymptotically in the limit $\ell \to 0$, using the Laplace and steepest descent methods, respectively. (Here, $\ell$ is the spatial scale associated with the velocity increments.) Note that Kalilasnath, Sreenivasan and Stolovitsky [16] have pursued a similar objective in terms of combining multifractal scaling with Gaussian statistics of a stochastic multiplier at the large scales to obtain the PDF of velocity increments. However, they did so using a specific multifractal model, without the benefit of a general asymptotic formula.

The paper is organized as follows. Section 2 is devoted to the theoretical background. We first derive the integral relations that link moments and PDF. Then the steepest descent and Laplace methods are used to evaluate the integrals. The dominant terms are shown to be equivalent to the Parisi–Frisch Legendre transform and the consistency of the sub-dominant terms is explicitly checked. The asymptotic relation is then used to generate PDF from known forms of the multifractal spectrum, assuming large scale Gaussian statistics.

Section 3 is concerned with the analysis of experimental data. We first briefly characterize the experimental setup and then apply our new algorithms to the data. The direct asymptotic relation (from PDF to moments) is used to reproduce the inertial-range moments. We then analyze the large scale moments and give an algorithm to determine the scale at which they are as close as possible to Gaussian. Small non-Gaussian corrections are then taken into account. The variation of the Gaussian scale with respect to Reynolds number is determined. The inverse asymptotic relation (from moments to PDF) is used to reconstruct the PDF. The experimental and reconstructed PDF are then compared. The reconstruction is also performed with values of the scaling exponents determined by analytic models.

Section 4 has the conclusions and the useful technical computations are given in the Appendix.

## 2. Theoretical background

### 2.1. Integral relations between moments and densities

As the velocity increments $v(x+\ell)-v(x)$ are of either sign, the structure functions which are closely related to their moments can be defined in several ways. In this paper, we have chosen to use the absolute values of the increments as in [17].

The $n$th order absolute value structure function is defined as

$$S(n,\ell)=\int_0^{+\infty} p_{\mathrm{inc}}(u,\ell)u^n\,\mathrm{d}u \tag{1}$$

where $u=|v(x+\ell)-v(x)|$ and $p_{\mathrm{inc}}$ is the associated probability density function (PDF). Defining the variable

$$\mathcal{L}_u=\log u \tag{2}$$

and the corresponding PDF $p(\mathcal{L}_u,\ell)=e^{\mathcal{L}_u}p_{\mathrm{inc}}(e^{\mathcal{L}_u},\ell)$, relation (1) can be written as

$$S(n,\ell)=\int_{-\infty}^{+\infty} e^{n\mathcal{L}_u}p(\mathcal{L}_u,\ell)\,\mathrm{d}\mathcal{L}_u \tag{3}$$

Note that the absolute value structure function $S(n,\ell)$ is well defined for non-integer values of $n$. We now define the characteristic function associated to $p(\mathcal{L}_u,\ell)$

$$Z(k,\ell)=\int_{-\infty}^{+\infty} e^{\mathrm{i}k\mathcal{L}_u}p(\mathcal{L}_u,\ell)\,\mathrm{d}\mathcal{L}_u \tag{4}$$

The characteristic function and the structure function are thus mathematically related as

$$S(n,\ell)=Z(-\mathrm{i}n,\ell) \tag{5}$$

$$Z(k,\ell)=S(\mathrm{i}k,\ell) \tag{6}$$

Using these relations, we can express the PDF as an inverse Fourier transform

$$p(\log u,\ell)=(2\pi)^{-1}\int_{-\infty}^{+\infty}\mathrm{e}^{-\mathrm{i}k\log u}S(\mathrm{i}k,\ell)\,\mathrm{d}k \tag{7}$$

Thus, the absolute value structure function evaluated for imaginary arguments is physically related to the characteristic function of the PDF in logarithmic variables.

### 2.2. Double asymptotic relation

We now suppose that the structure functions follow scaling laws with multifractal exponents $\zeta_n$, for $\ell<\ell_G$

$$S(n,\ell)=A_n\left[\frac{\ell}{\ell_G}\right]^{\zeta_n} \tag{8}$$

where $\ell_G$ is an arbitrary scale $\ell_G>\ell$ at this point. Factoring out the $\log(\ell/\ell_G)$ term, we can write the integral relations (3) and (7) in a form suitable to their asymptotic evaluation. Relation (3), with the notation $\log u=\mathcal{L}_u=h\log(\ell/\ell_G)$, gives

$$S(n,\ell)=-\log\left(\frac{\ell}{\ell_G}\right)\int_{-\infty}^{+\infty}\exp\left\{\log\left(\frac{\ell}{\ell_G}\right)\left[nh+\frac{\log p\,(h\log(\ell/\ell_G),\ell)}{\log(\ell/\ell_G)}\right]\right\}\mathrm{d}h \tag{9}$$

and Eq. (7) yields

$$p\left(h\log\left(\frac{\ell}{\ell_G}\right),\ell\right)=(2\pi)^{-1}\int_{-\infty}^{+\infty}\exp\left\{\log\left(\frac{\ell}{\ell_G}\right)\left[-\mathrm{i}kh+\frac{\log S(\mathrm{i}k,\ell)}{\log(\ell/\ell_G)}\right]\right\}\mathrm{d}k \tag{10}$$

We define the following functions

$$\mu(h,\ell)=\frac{\log p\left(h\log(\ell/\ell_G),\ell\right)}{\log(\ell/\ell_G)} \tag{11}$$

$$\zeta(n,\ell)=\frac{\log S(n,\ell)}{\log(\ell/\ell_G)} \tag{12}$$

and let us assume that they admit finite $\ell\to 0$ limits

$$\lim_{\ell\to 0}\mu(h,\ell)=\mu(h) \tag{13}$$

$$\lim_{\ell\to 0}\zeta(n,\ell)=\zeta_n \tag{14}$$

Note that the finite $\ell\to 0$ limit of Eq. (13) is equivalent to the probabilistic reformulation of Frisch (see [6] p. 147, relation (8.50)). The finite $\ell\to 0$ limit of Eq. (12) is a simple consequence of Eq. (8).

*2.2.1. Steepest descent method*

The steepest descent method applied to Eq. (10) (see Appendix A.2) gives the relations

$$h(n,\ell)=\frac{1}{\log(\ell/\ell_G)}\frac{\partial\log S(n,\ell)}{\partial n} \tag{15}$$

$$\log p(n,\ell)=-n\frac{\partial\log S(n,\ell)}{\partial n}+\log S(n,\ell)-\frac{1}{2}\log(2\pi)-\frac{1}{2}\log\left[\frac{\partial^2\log S(n,\ell)}{\partial n^2}\right]+\mathcal{O}\left[\frac{1}{\log(\ell/\ell_G)}\right] \tag{16}$$

or equivalently, using the variable $\mathcal{L}_u\equiv\log u=h\log(\ell/\ell_G)$, Eq. (15) reads

$$\log u(n,\ell)=\frac{\partial\log S(n,\ell)}{\partial n} \tag{17}$$

Eqs. (16) and (17) give a parametric representation of the logarithm of the PDF $p(\mathcal{L}_u,\ell)$, with parameter $n$. Inverting Eq. (17) to obtain an expression for $n=n(\mathcal{L}_u,\ell)$ and inserting this expression into Eq. (16) yields $p(\mathcal{L}_u,\ell)$.

*2.2.2. Laplace method*

Evaluating Eq. (9) by the Laplace method (see Appendix A.1) gives the following relations

$$n(h,\ell)=-\frac{1}{\log(\ell/\ell_G)}\frac{\partial\log p\left(h\log(\ell/\ell_G),\ell\right)}{\partial h} \tag{18}$$

$$\begin{aligned}\log S(h,\ell)=&-\frac{\partial\log p\left(h\log(\ell/\ell_G),\ell\right)}{\partial h}h+\log p\left(h\log(\ell/\ell_G),\ell\right)+\frac{1}{2}\log(2\pi)\\&-\frac{1}{2}\log\left[-\frac{\partial^2\log p\left(h\log(\ell/\ell_G),\ell\right)}{\partial h^2}\right]+\log\left[-\log\left(\frac{\ell}{\ell_G}\right)\right]+\mathcal{O}\left[\frac{1}{\log(\ell/\ell_G)}\right]\end{aligned} \tag{19}$$

or equivalently, using the variable $\mathcal{L}_u\equiv\log u=h\log(\ell/\ell_G)$

$$n(\log u,\ell)=-\frac{\partial\log p(\log u,\ell)}{\partial\log u} \tag{20}$$

$$\log S(\log u, \ell) = -\frac{\partial \log p(\log u, \ell)}{\partial \log u} \log u + \log p(\log u, \ell) + \frac{1}{2}\log(2\pi) - \frac{1}{2}\log\left[-\frac{\partial^2 \log p(\log u, \ell)}{\partial \log u^2}\right] + \mathcal{O}\left[\frac{1}{\log(\ell/\ell_G)}\right] \tag{21}$$

Eqs. (20) and (21) give a parametric representation of the logarithm of the structure function $S(n, \ell)$, with parameter $\mathcal{L}_u$. Inverting Eq. (20) to obtain an expression for $\mathcal{L}_u = \mathcal{L}_u(n, \ell)$ and inserting this expression into Eq. (21) yields $S(n, \ell)$.

### 2.3. Parisi–Frisch Legendre transform

We now show that the dominant exponential terms of Eqs. (16), (17), (20) and (21) are equivalent to the Parisi–Frisch Legendre transform. To wit, inserting Eq. (12) into Eq. (15) we get

$$h(n, \ell) = \frac{\partial \zeta(n, \ell)}{\partial n} \tag{22}$$

Furthermore, we define the function

$$\bar{\mu}(n, \ell) = \frac{\log p(n, \ell)}{\log(\ell/\ell_G)} \tag{23}$$

and from Eq. (16), we obtain

$$\bar{\mu}(n, \ell) = -n\frac{\partial \zeta(n, \ell)}{\partial n} + \zeta(n, \ell) - \frac{1}{\log(\ell/\ell_G)}\left\{\frac{1}{2}\log(2\pi) + \frac{1}{2}\log\left[\log\left(\frac{\ell}{\ell_G}\right)\frac{\partial^2 \zeta(n, \ell)}{\partial n^2}\right]\right\} + \mathcal{O}\left[\frac{1}{\log(\ell/\ell_G)^2}\right] \tag{24}$$

Using Eqs. (8) and (12), we obtain

$$\zeta(n, \ell) = \zeta_n + \frac{\log A_n}{\log(\ell/\ell_G)} + \mathcal{O}\left[\frac{1}{\log(\ell/\ell_G)^2}\right] \tag{25}$$

We now take the $\ell \to 0$ limit of expressions (22) and (24) using Eq. (14) and uniformity in $n$. With the notations

$$\lim_{\ell \to 0} h(n, \ell) = h_n \tag{26}$$

$$\lim_{\ell \to 0} \bar{\mu}(n, \ell) = \bar{\mu}_n \tag{27}$$

Eqs. (22) and (24) yield

$$h_n = \frac{\mathrm{d}\zeta_n}{\mathrm{d}n}$$

$$\bar{\mu}_n = -nh_n + \zeta_n$$

which is the inverse Legendre transform of the Parisi–Frisch model (see Fig. 1).

The direct Parisi–Frisch Legendre transform is obtained in the following way. Inserting Eq. (11) into Eq. (19) and defining the function

$$\bar{\zeta}(h, \ell) = \frac{\log S(h, \ell)}{\log(\ell/\ell_G)} \tag{28}$$

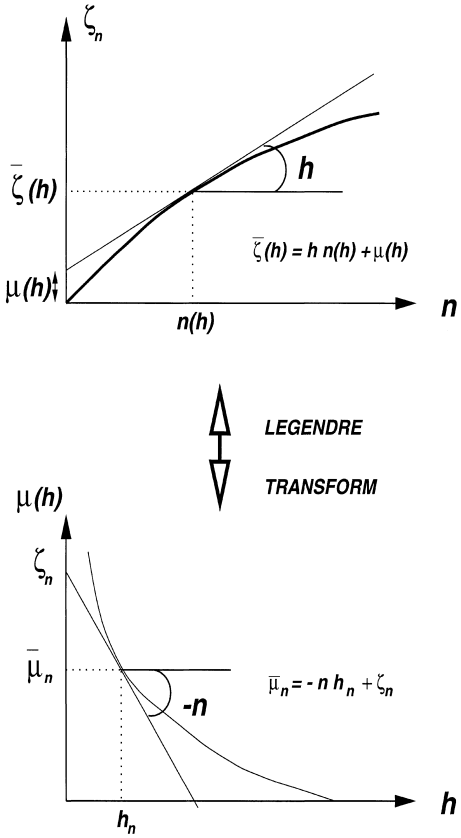


Fig. 1. The Parisi–Frisch Legendre transform.

gives the relations

$$n(h,\ell) = -\frac{\partial \mu(h,\ell)}{\partial h} \tag{29}$$

$$\bar{\zeta}(h,\ell) = -\frac{\partial \mu(h,\ell)}{\partial h} h + \mu(h,\ell) + \frac{1}{\log(\ell/\ell_G)} \left\{ \frac{1}{2}\log(2\pi) - \frac{1}{2}\log\left[ -\frac{1}{\log(\ell/\ell_G)} \frac{\partial^2 \mu(h,\ell)}{\partial h^2} \right] \right\} + \mathcal{O}\left[ \frac{1}{\log(\ell/\ell_G)^2} \right] \tag{30}$$

We now take the $\ell \to 0$ limit of expressions (29) and (30), using Eq. (13) and uniformity in $h$. With the notations

$$\lim_{\ell \to 0} n(h,\ell) = n(h) \tag{31}$$

$$\lim_{\ell \to 0} \bar{\zeta}(h,\ell) = \bar{\zeta}(h) \tag{32}$$

Eqs. (29) and (30) yield

$$n(h) = -\frac{\mathrm{d}\mu(h)}{\mathrm{d}h}$$

$$\bar{\zeta}(h) = n(h)h + \mu(h)$$

which is the direct Legendre transform of the Parisi–Frisch model (see Fig. 1).

Thus, the Legendre transform that is central to the Parisi–Frisch model is naturally contained in the double asymptotic relations (16) and (19), at the dominant level. Relations (22) and (29) are the extremum conditions.

### 2.4. Consistency of the sub-dominant terms

The consistency of the dominant terms in the double asymptotic relation is a consequence of the involution property of the Legendre transform. We now proceed to show that this involutive property extends to the nondominant terms.

We can express the scaling laws (8) in the logarithmic form as

$$\log S(n,\ell) = \log A_n + \zeta_n \log\left(\frac{\ell}{\ell_G}\right) \tag{33}$$

Relations (16) and (17) give the following expressions for the PDF

$$\log u(n,\ell) = \log\left(\frac{\ell}{\ell_G}\right)\frac{\mathrm{d}\zeta_n}{\mathrm{d}n} + \frac{\mathrm{d}\log A_n}{\mathrm{d}n} + \mathcal{O}\left[\frac{1}{\log(\ell/\ell_G)}\right] \tag{34}$$

$$\begin{aligned}\log p(n,\ell) = {}& \log\left(\frac{\ell}{\ell_G}\right)\left[\zeta_n - n\frac{\mathrm{d}\zeta_n}{\mathrm{d}n}\right] + \log A_n - n\frac{\mathrm{d}\log A_n}{\mathrm{d}n} - \frac{1}{2}\log(2\pi) - \frac{1}{2}\log\left[\log\left(\frac{\ell}{\ell_G}\right)\frac{\mathrm{d}^2\zeta_n}{\mathrm{d}n^2}\right] \\ & + \mathcal{O}\left[\frac{1}{\log(\ell/\ell_G)}\right]\end{aligned} \tag{35}$$

In order to check the involution property at the sub-dominant level, we want to use these parametric expressions of the PDF to recover the moments using Eqs. (20) and (21). To do so, we first need to compute the first and second derivatives of the probability density $\log p(\mathcal{L}_u, \ell)$ from Eqs. (34) and (35). We get

$$\begin{aligned}\frac{\partial \log p(\log u,\ell)}{\partial \log u} &= \frac{\partial \log p(n,\ell)}{\partial n}\left[\frac{\partial \log u(n,\ell)}{\partial n}\right]^{-1} \\ &= -n - \frac{1}{2\log(\ell/\ell_G)}\frac{\mathrm{d}^3\zeta_n}{\mathrm{d}n^3}\left[\frac{\mathrm{d}^2\zeta_n}{\mathrm{d}n^2}\right]^{-1} + \mathcal{O}\left[\frac{1}{\log(\ell/\ell_G)^2}\right]\end{aligned} \tag{36}$$

and

$$\begin{aligned}\frac{\partial^2 \log p(\log u,\ell)}{\partial \log u^2} &= \frac{\partial}{\partial n}\left\{\frac{\partial \log p(n,\ell)}{\partial n}\left[\frac{\partial \log u(n,\ell)}{\partial n}\right]^{-1}\right\}\left[\frac{\partial \log u(n,\ell)}{\partial n}\right]^{-1} \\ &= -\frac{1}{\log(\ell/\ell_G)}\left[\frac{\mathrm{d}^2\zeta_n}{\mathrm{d}n^2}\right]^{-1} + \mathcal{O}\left[\frac{1}{\log(\ell/\ell_G)^2}\right]\end{aligned} \tag{37}$$

Inserting Eqs. (34)–(36) into Eq. (20) gives for the order of the computed moment, the expression

$$n_s(n,\ell) = n + \frac{1}{2\log(\ell/\ell_G)}\frac{\mathrm{d}^3\zeta_n}{\mathrm{d}n^3}\left[\frac{\mathrm{d}^2\zeta_n}{\mathrm{d}n^2}\right]^{-1} + \mathcal{O}\left[\frac{1}{\log(\ell/\ell_G)^2}\right] \tag{38}$$

In the same way, inserting Eqs. (34)–(37) into Eq. (21) gives for the value of the structure function of order $n_s(n,\ell)$, the expression

$$\log S(n,\ell) = \log A_n + \log\left[\frac{\ell}{\ell_G}\right]\zeta_n + \frac{1}{2}\frac{\mathrm{d}^3\zeta_n}{\mathrm{d}n^3}\frac{\mathrm{d}\zeta_n}{\mathrm{d}n}\left[\frac{\mathrm{d}^2\zeta_n}{\mathrm{d}n^2}\right]^{-1} + \mathcal{O}\left[\frac{1}{\log(\ell/\ell_G)}\right] \tag{39}$$

Table 1
Multifractal models of exponents $\zeta_n$

| Models | Exponents | Parameters |
|---|---|---|
| Log-normal | $\zeta_n = n/3 + \eta(3n - n^2)/18$ | $\eta = 0.2$ |
| She-Lévêque | $\zeta_n = n/9 + 2(1 - (2/3)^{n/3})$ | No parameters |

Let us first remark that the sub-dominant $\log(-\log(\ell/\ell_G))$ terms present in Eqs. (24) and (30) have cancelled out in Eq. (39). To check the involution property at the sub-dominant level, it is enough to further remark that Taylor expanding in $n$ the structure function (33) to order $n_s$ given by Eq. (38) yields expression (39).

To close this section, note that it is possible to compute higher-order terms in the asymptotic relations (see Appendix A.3) and also check their involutive property [18]. However, we will not need to use these higher-order terms in the rest of this paper. Also, note that the higher-order formulae involve higher-order derivatives of the PDF and structure functions. This raises the problem of error propagation. If one looks back at the derivation of the double asymptotic relation (see Section 2.2 and Appendix A.1), one can see that the direct formulae (20) and (21) are a straightforward application of the Laplace method [19], while the inverse formulae (16) and (17), first involves an analytic continuation. Thus, the problem of error propagation in the double asymptotic relation is nontrivial. However, as will be shown below in Section 3, in the practical case of experimental turbulent data, the errors are small when using the lowest-order approximation.

### 2.5. Large scale Gaussian (LSG) hypothesis

In order to compute practically the PDF using the asymptotic expressions (16) and (17), we need an expression for the moments $A_n$ at the large scale $\ell_G$ defined in Eq. (8). We now suppose that at scale $\ell_G$, the moments are those corresponding to a Gaussian distribution with standard deviation $u_G$

$$\frac{1}{\sqrt{\pi/2}u_G}\int_0^{+\infty} \mathrm{e}^{-x^2/2u_G^2}\, x^n \,\mathrm{d}x = \frac{1}{\sqrt{\pi}}\Gamma\left[\frac{n+1}{2}\right]\left[\sqrt{2}u_G\right]^n$$

Thus, the $A_n$ term in expression (8) has the value

$$\log A_n = \log\left\{\Gamma\left[\frac{n+1}{2}\right]\left[\sqrt{2}u_G\right]^n\right\} - \frac{1}{2}\log\pi \tag{40}$$

The LSG hypothesis is the explicit expression for the structure function obtained from Eqs. (8) and (40)

$$\log S(n,\ell) = \log\left\{\Gamma\left[\frac{n+1}{2}\right]\left[\sqrt{2}u_G\right]^n\right\} - \frac{1}{2}\log\pi + \zeta_n \log\left[\frac{\ell}{\ell_G}\right] \tag{41}$$

The LSG hypothesis (41) provides a complete determination, using Eq. (16) and (17) of the PDF in terms of the multifractal exponents $\zeta_n$ and the Gaussian scales $\ell_G$ and $u_G$. In the rest of this paper, we will call this explicit determination of the PDF, the multifractal asymptotic model (MAM).

The MAM PDF corresponding to the log-normal and the She-Lévêque models (see Table 1 ) are shown in Fig. 2 , for $\ell/\ell_G = 1/4, 1/16, 1/64, 1/512$, $u_G = 1$ and $n = 1, \ldots, 16$.

Figs. 2(A,B) show the values of $\log u$ and $\log p$ as a function of the parameter $n$. The reconstructed PDF as a function of $\log u$ obtained by inverting the relation shown in Fig. 2(A), is presented in Fig. 2(C). The PDF as a function of $u$ is plotted in Fig. 2(D).

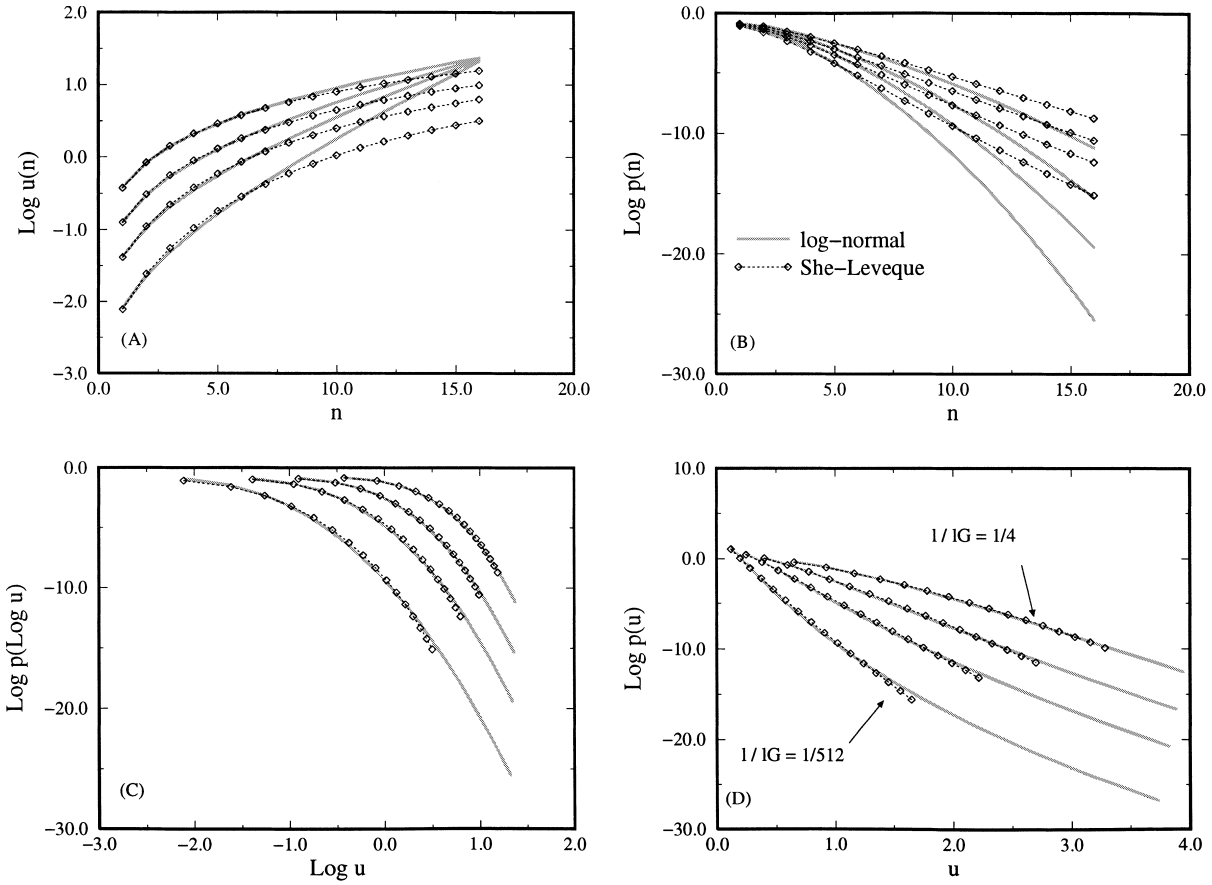


Fig. 2. Reconstruction of the PDF using the MAM Eqs. (16), (17) and (41) for different models (see Table 1) at scales $\ell/\ell_G = 1/4, 1/16, 1/64, 1/512$. (A) $\log u(n, \ell)$ as a function of the parameter $n$. (B) $\log p(n, \ell)$ as a function of the parameter $n$. (C) Classical representation of $\log p(\log u, \ell)$. (D) Classical representation of $\log p(u, \ell)$.

Note that, it can be seen from Fig. 2(D) that the form of the PDF changes when the scale is modified. This is a characteristic of multifractal scaling in contrast to unifractal scaling, where one expects to find a (re-scaled) invariant form for the PDF.

## 3. Analysis of experimental data

### *3.1. Characteristic of experimental data*

We have used the experimental setup that is described in detail in [20–22]. Schematically, a low temperature flow of helium gas is confined in a cylinder which is limited axially by disks equipped with blades. The turbulence is produced by rotating the two disks in opposite direction. The local velocity is measured by a hot-wire anemometer made from a carbon fiber of thickness 7 μm. It is possible to obtain a large spectrum of Taylor-scale Reynolds number ($R_\lambda$ from 300 to 2200) by controlling the temperature $T$ (from 4.2 to 8 K) and the pressure $P$ (from $10^{-2}$ to 3 atm). In this paper, we have analyzed several experimental runs that are summarized in Table 2. The experiment '69A78'

Table 2
Physical characteristics of the experimental data. $\langle U\rangle$: mean velocity, $f_s$: sample frequency, $\ell_e = \langle U\rangle/f_s$: sample scale and $\ell_I$: integral scale.

| File | V148 | V143 | V140 | V97 | V133 | 69A78 | V156 | V157 |
|---|---|---|---|---|---|---|---|---|
| $R_\lambda$ | 302 | 391 | 465 | 747 | 1204 | 2000 | 1600 | 2200 |
| $\langle U\rangle$(cm/s) | 228 | 36.3 | 63 | 63.2 | 108.2 | 129 | 128.5 | 128.5 |
| $f_s$(kHz) | 15.625 | 7.812 | 15.625 | 31.25 | 31.25 | 125 | 125 | 125 |
| $\ell_e(10^{-3}$ cm) | 14.6 | 4.6 | 4 | 2 | 3.456 | 1.56 | 1 | 1 |
| $\ell_I$(cm) | 2.2 | 1.66 | 1.54 | 1.77 | 0.96 | 4 | 1.64 | 3.55 |

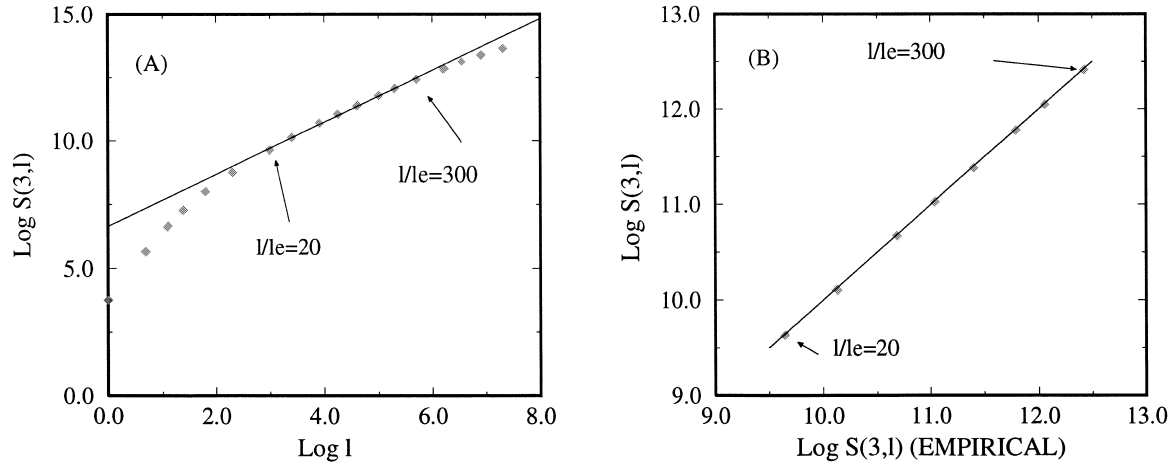


Fig. 3. (A) Determination of the inertial range $20\ell_e \le \ell \le 300\ell_e$ for the '69A78' file (see Table 2). (B) Validity of the direct asymptotic method Eqs. (20) and (21) for $S(3, \ell)$ with $\ell$ in the inertial range.

includes 9 distinct samples of $10^9$ velocimetry data points. The other experiments include $3 \times 10^7$ velocimetry data points.

By now, a standard way to analyze the scaling of experimental turbulent data is the extended self similarity (ESS) method [17]. In this method, the scaling of the $n$th order structure function is determined against the scaling of the third order structure function. We have used the ESS method inside the inertial range in order to be able to compare the scaling exponents with previously published data (see Table 2). Using the '69A78' dataset, a fit of the third order structure function in the range $20\ell_e < \ell < 300\ell_e$ gives an exponent equal to 1 with precision $10^{-3}$ (see Fig. 3 (A)). The values of $\zeta_n$ for $n \neq 3$ are determined by fitting the structure functions, with respect to the third order structure function, within this range. This procedure amounts to using a length scale $\ell_{\mathrm{ESS}}$ proportional to the third-order structure function $S_3(\ell)$ inside the inertial range. The detailed determination of $\ell_{\mathrm{ESS}}$ is described below.

### 3.2. Test of direct method and determination of $\mu(h)$

As a first test of the validity of the asymptotic relation (21), we have checked that Eq. (21) gave correct values for $S(3, \ell)$ with $\ell$ in the inertial range.

For each value of $\ell$, the moment $S(3, \ell)$ is obtained by our method, by determining the value of $\log u$ that gives $n = 3$ in Eq. (20) and inserting this value in Eq. (21). It can be checked in Fig. 3(B) that this procedure correctly reproduces the empirical $S(3, \ell)$.

The direct asymptotic relations (20) and (21) can be used to compute the Parisi–Frisch functions $\mu(h)$ and $\zeta_n$ [23]. This can be achieved in three steps as first derived in [23].

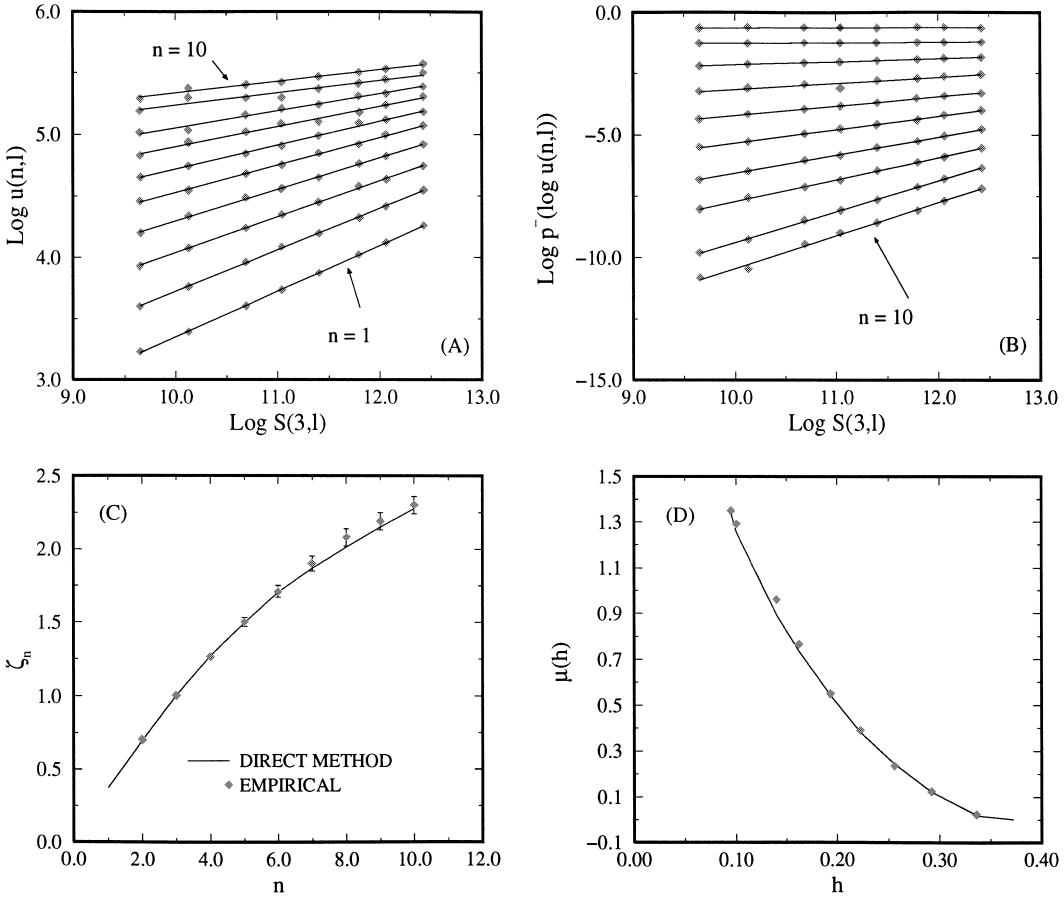


Fig. 4. (A) $\log u(n,\ell)$ versus $\log S(3,\ell)$ for $n = 1,\ldots,10$. The scaling law (42), displayed as straight lines gives $h_n$ as the slope. (B) $\log p(\log u,\ell) + (1/2)\log(2\pi) - (1/2)\log\left[-\partial^2 \log p(\log u,\ell)/\partial \log u^2\right]$ versus $\log S(3,\ell)$ for $n = 1,\ldots,10$. The scaling law (43), displayed as straight lines gives the codimension $\mu_n$ as the slope. (C) $\zeta_n$ determined by scaling law (44) and experimental $\zeta_n(\diamond)$. (D) $\mu(h)$ determined by scaling laws (42) and (43) (see (A,B)) and experimental $\mu(h)$ determined by Legendre transform of experimental $\zeta_n$ (see (C))($\diamond$).

Each of the three steps involves the determination of a power law by linear fits in log–log coordinates. In order to agree with previously published data obtained by the ESS methods, the power law is determined with respect to the ESS length scale $\ell_{\mathrm{ESS}}$. This length scale is determined by the following procedure. First, $\log S(3,\ell)$ is fit inside the inertial range by a linear law $\log S_{\mathrm{lin}}(3,\ell) = \log \ell + C^{\mathrm{te}}$. Then, $\ell_{\mathrm{ESS}}$ is defined by the formula $\log \ell_{\mathrm{ESS}} = \log S_{\mathrm{lin}}(3,\ell) - \log S_{\mathrm{lin}}(3,\ell_e) + \log \ell_e$. Note that we are performing such ESS fits within the inertial range (see Fig. 3(A)).

The Parisi–Frisch functions are determined as follows. In the first step, inverting Eq. (20) for several values of $n$, the function $h_n$ is determined by linear fits over the inertial range of the form

$$\log u(n,\ell_{\mathrm{ESS}}) = h_n \log \ell_{\mathrm{ESS}} + C_1(n) \tag{42}$$

(see Fig. 4 (A)). In the second step, substituting into Eq. (21) the $\log u$ value obtained in the first step and fitting the corresponding $\log S$ values with the linear expression

$$\log S(n,\ell_{\mathrm{ESS}}) = \zeta_n \log \ell_{\mathrm{ESS}} + C_2(n) \tag{43}$$

determines $\zeta_n$. Finally, using the Parisi–Frisch Legendre transform $\zeta_n = h_n n + \mu_n$ and Eq. (21), $\mu_n$ can be determined by the linear fit

$$\log \bar{p}(\log u(n, \ell_{\mathrm{ESS}}), \ell_{\mathrm{ESS}}) = \mu_n \log \ell_{\mathrm{ESS}} + C_3(n)$$

where

$$\log \bar{p}(\log u(n, \ell_{\mathrm{ESS}}), \ell_{\mathrm{ESS}}) = \log p(\log u(n, \ell_{\mathrm{ESS}}), \ell_{\mathrm{ESS}}) + \frac{1}{2}\log(2\pi) - \frac{1}{2}\log\left[-\frac{\partial^2 \log p(\log u, \ell_{\mathrm{ESS}})}{\partial \log u^2}\right] \tag{44}$$

(see Fig. 4(B)). Thus, it is apparent that the direct asymptotic formula Eq. (21) give satisfactory results in the inertial range (see Figs. 4(C,D)).

### *3.3. Determination of the Gaussian scale*

We now turn to the determination of the Gaussian scale $\ell_G$. A general multifractal scaling law of the form

$$\log S(n, \ell) = C_n + \zeta_n \log \ell \tag{45}$$

can be written as Eq. (33) with

$$\log A_n = C_n + \zeta_n \log \ell_G \tag{46}$$

Starting from Eq. (45), we seek a length scale $\ell_G$ such that $A_n$ determined by Eq. (46) can be considered to be Gaussian moments and thus obey Eq. (40). Defining

$$\mathcal{F}(n) = C_n + \zeta_n \log \ell_G - \log \Gamma\left[\frac{n+1}{2}\right] + \frac{1}{2}\log \pi \tag{47}$$

for each value of $\ell_G$, one fits $\mathcal{F}(n)$ over some range $n$ with a quadratic polynomial

$$\mathcal{P}(n) = An + Bn^2 \tag{48}$$

$\ell_G$ is determined when $B = 0$. $u_G$ is then given by the relation $A = \left[\log u_G + (1/2)\log 2\right]$. In practice, once $\ell_G$ is determined, the function $\mathcal{F}(n)$ will not be exactly linear. The small nonlinearities of $\mathcal{F}(n)$ can be taken into account by using a higher-order polynomial (arbitrarily taken as order five)

$$\mathcal{P}(n) = \left[\log u_G + \frac{1}{2}\log 2\right] n + Bn^2 + Cn^3 + Dn^4 + En^5 \tag{49}$$

In the rest of this paper, we will refer to the statistics of the large scales when the small non-Gaussian corrections are taken into account as large scale quasi Gaussian (LSQG). In this case, the moments can be written as

$$\log S(n, \ell) = \log \Gamma\left[\frac{n+1}{2}\right] - \frac{1}{2}\log \pi + \zeta_n \log\left(\frac{\ell}{\ell_G}\right) + \mathcal{P}(n) \tag{50}$$

The quality of the representation of the structure functions at the scale $\ell_G$ by the LSG (41) and LSQG (50) formulae is shown in Fig. 5. An error bar for the determination of $\ell_G$ can be obtained in the following way. For each value of $n$, when

$$\frac{\mathrm{d}^2 C_n}{\mathrm{d}n^2} + \frac{\mathrm{d}^2 \zeta_n}{\mathrm{d}n^2} \log \ell_G = \frac{\mathrm{d}^2 \log \Gamma\left((n+1)/2\right)}{\mathrm{d}n^2}$$

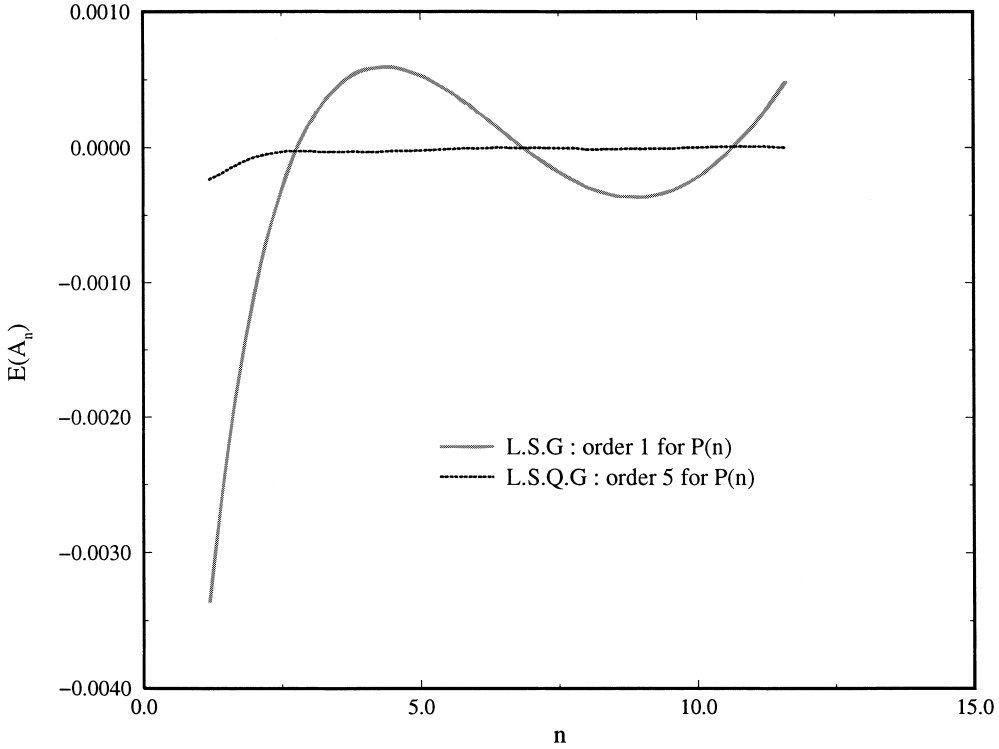


Fig. 5. Relative error $E(A_n) = (\log A_n - \mathcal{P}(n) - \log\Gamma[(n+1)/2] + (1/2)\log\pi)/\log A_n$ with $\mathcal{P}(n)$ given by LSG Eq. (48) and LSQG Eq. (49), for the '69A78' dataset (see Table 2).

yields

$$\log \ell_G = \frac{1}{\mathrm{d}^2\zeta_n/\mathrm{d}n^2}\left\{\frac{\mathrm{d}^2 \log\Gamma\left((n+1)/2\right)}{\mathrm{d}n^2} - \frac{\mathrm{d}^2 C_n}{\mathrm{d}n^2}\right\} \tag{51}$$

We determine the error bar by taking the minimum and maximum of Eq. (51) over the considered range $n$.

Note that the determination of $\ell_G$ and $u_G$ is obtained from inertial range data. It is interesting to see, how these quantities scale with the Reynolds number. The results and fit displayed in Fig. 6 show that $\ell_G$ and $u_G$ remain close to the integral scale quantities $\ell_I$ and $u_I$. It can be seen by inspection of the figure that, although the error bars are very wide (over a factor of five), no systematic trend is apparent in the studied range of Taylor-scale Reynolds numbers. Thus, the algorithm for the determination of $\ell_G$ is able to yield correct values, within a large scatter, for the integral scale from intermittency data in the inertial range. This strongly supports the notion of intermittency corrections arising from a cascade process that begins at the integral scale.

### *3.4. Reconstruction of the probability density function (inverse method) and validity test of simple analytic expressions*

We now proceed to see, how well the LSG (41) and LSQG (50) representations together with the inverse asymptotic relation (16) are able to reconstruct the probability density functions. The PDF are shown in Fig. 7 in the parametric form defined in Section 2.2, Eqs. (20) and (21). In Fig. 8 , the PDF are shown in the standard form as functions of $u$ or $\log u$. It is apparent from Figs. 7(B,D) that the tails of the PDF are in better quantitative agreement when

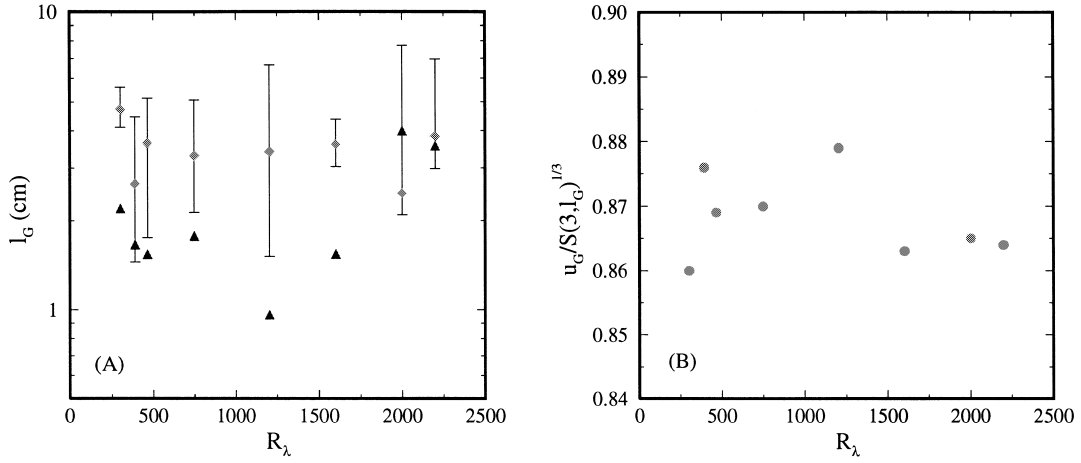


Fig. 6. Gaussian scale $\ell_G$ as a function of the Reynolds number $R_\lambda$. The scale $\ell_G$ is displayed by ($\diamond$), the error bars are determined by Eq. (51). The integral scale is displayed by ($\triangle$). (B) Ratio $u_G/S(3, \ell_G)^{1/3}$.

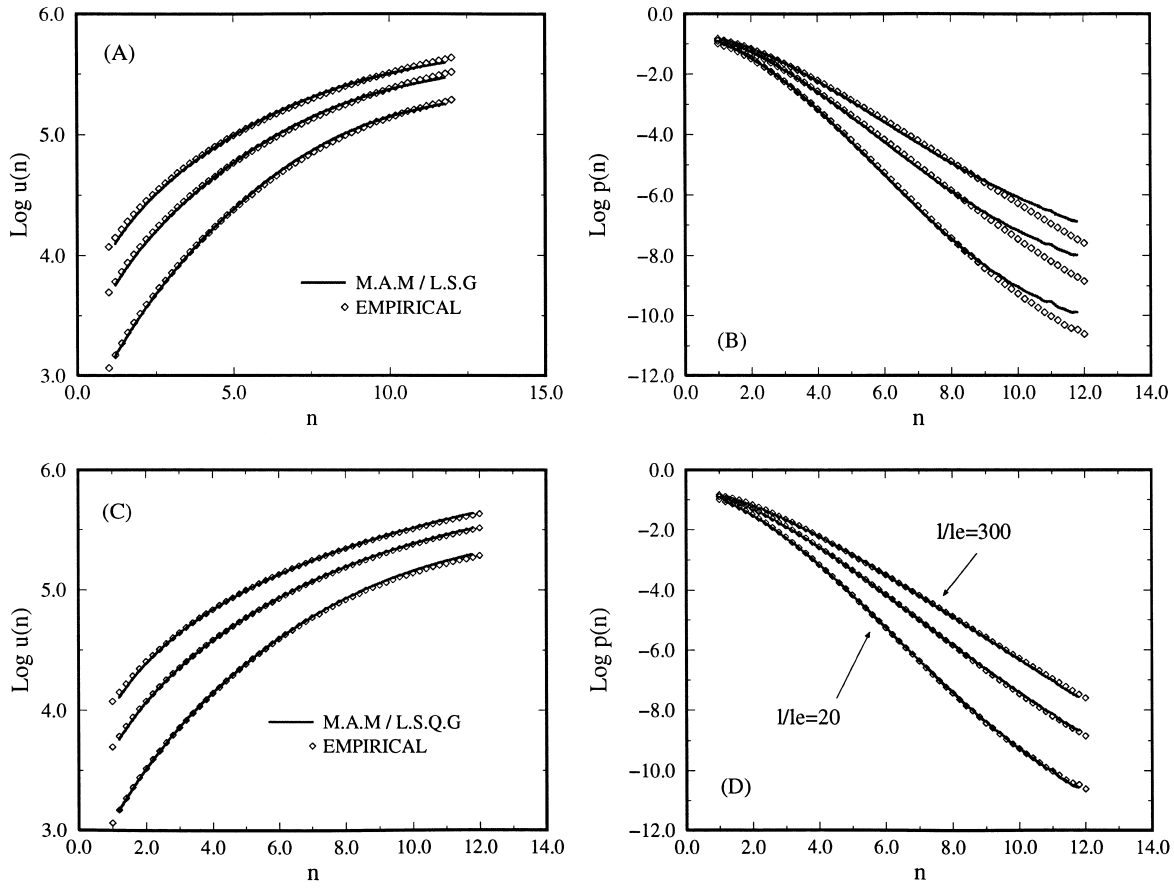


Fig. 7. Parametric representation of the PDF Eqs. (20) and (21) using the LSG (41) (see (A,B)) and LSQG (50) (see (C,D)) representations with $\ell/\ell_e = 20, 100, 300$.

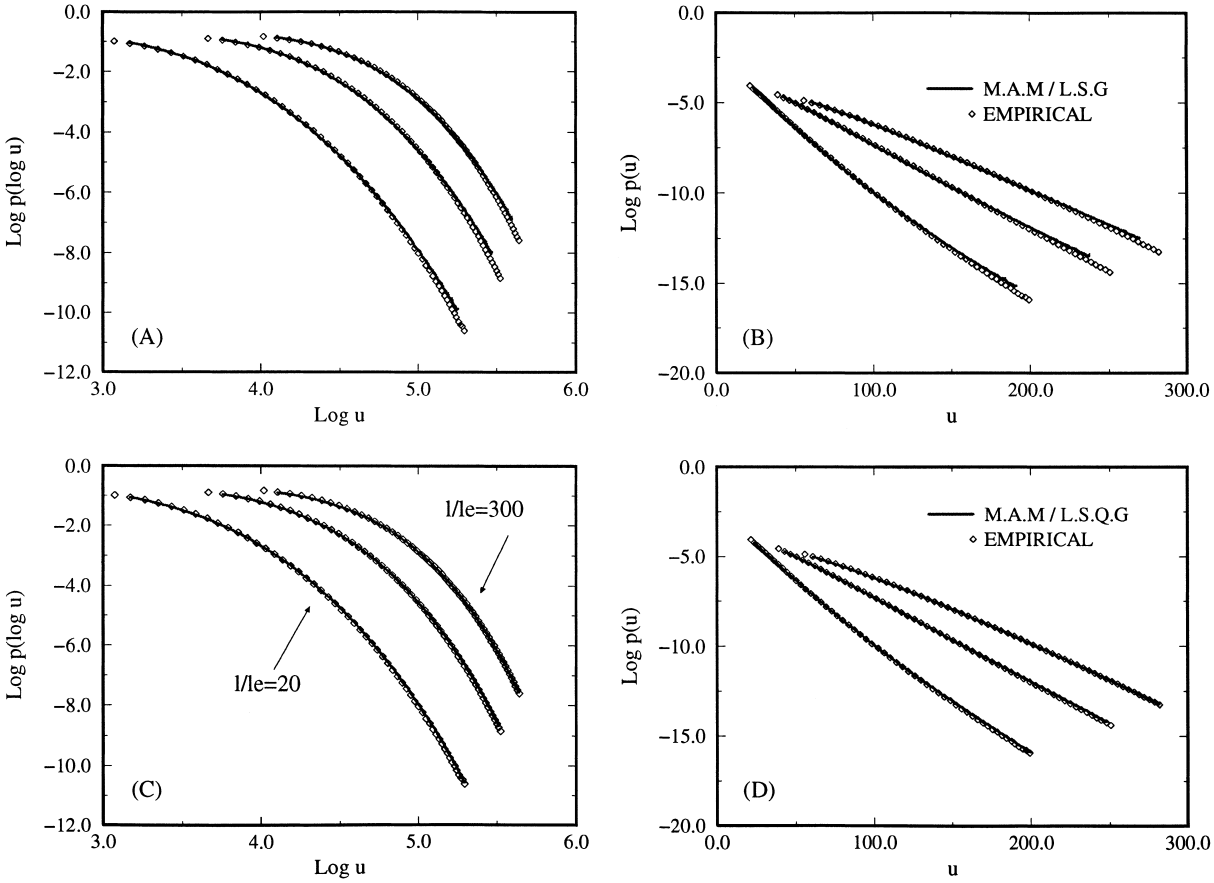


Fig. 8. Same data as in Fig. 7, with log $p$ using the LSG representation plotted as function of log $u$ (see (A)) or as function of $u$ (see (B)). Same plot with LSQG representation (see (C,D)).

the LSQG corrections are taken into account. We have thus shown that the experimentally determined exponent $\zeta_n$ together with the LSG or LSQG representation are able to quantitatively represent the experimental PDF.

It is interesting to see, if simple analytical expressions for $\zeta_n$, such as the log-normal and She-Lévêque, are also able to represent the data. This seems to be a somewhat more stringent test of the analytic expressions than just comparing their predictions with experimental values of $\zeta_n$.

The probabilities generated by the She-Lévêque and log-normal models are compared with the experimental data at a Taylor-scale Reynolds number of 2000 in Figs. 9 and 10 . Fig. 9 shows the parametric representation of log $u$ (Eq. (17)) and Fig. 10 shows the parametric representation of log $p$ (Eq. (16)). It is apparent from the figures that both the She-Lévêque and log-normal expressions yield systematic deviations from the experimental data of the inertial-range PDF at Taylor-scale Reynolds number $R_\lambda = 2000$.

## 4. Conclusions

To summarize, the main results obtained in this paper are

- The LSG (41) and LSQG (50) representations together with the inverse asymptotic relation (16) are able to reconstruct the probability density functions.

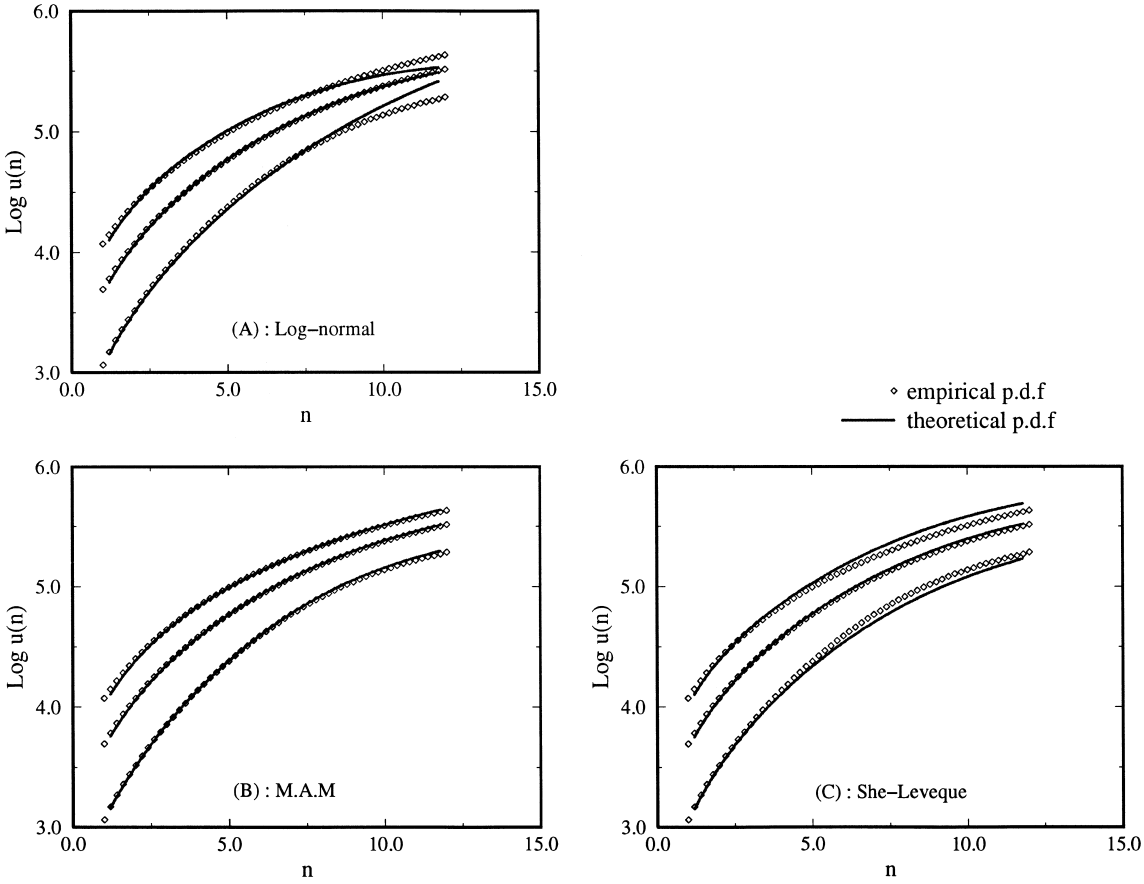


Fig. 9. Parametric plot of $\log u(n, \ell)$ for (A) log-normal model, (B) MAM model, (C) She-Lévêque model.

- The large scale $\ell_G$, determined from inertial-range data, is close to the integral scale for a large range of Reynolds numbers.
- The probabilistic reformulation of the Parisi–Frisch model is naturally contained in the asymptotic relations at the level of the dominant exponential terms.
- The procedure is in good agreement with experimental data, provided that the LSQG statistics are used together with the experimentally determined $\zeta_n$. The agreement deteriorates significantly, if both the conditions are not satisfied.

Note that the MAM procedures (16), (17) and (41) can be applied to fields other than turbulence, provided that the large scale statistics are Gaussian and multifractal scaling laws are present. Such is the case for exchange rate fluctuations in finance (see [18]).

Two points have been left for future work. First, it seems possible to extend the description to (separately) both negative and positive velocity increments. To do this, one should work with the PDF of negative and positive increments $p^{\pm}_{\mathrm{inc}}(u, \ell)$ and the corresponding moments as done in [6]. Second, it would be interesting to see if the MAM can be extended to describe the fluctuations of energy dissipation. The nontrivial problem is then to find a description of large scale statistics that could play a role equivalent to that of the LSG hypothesis.

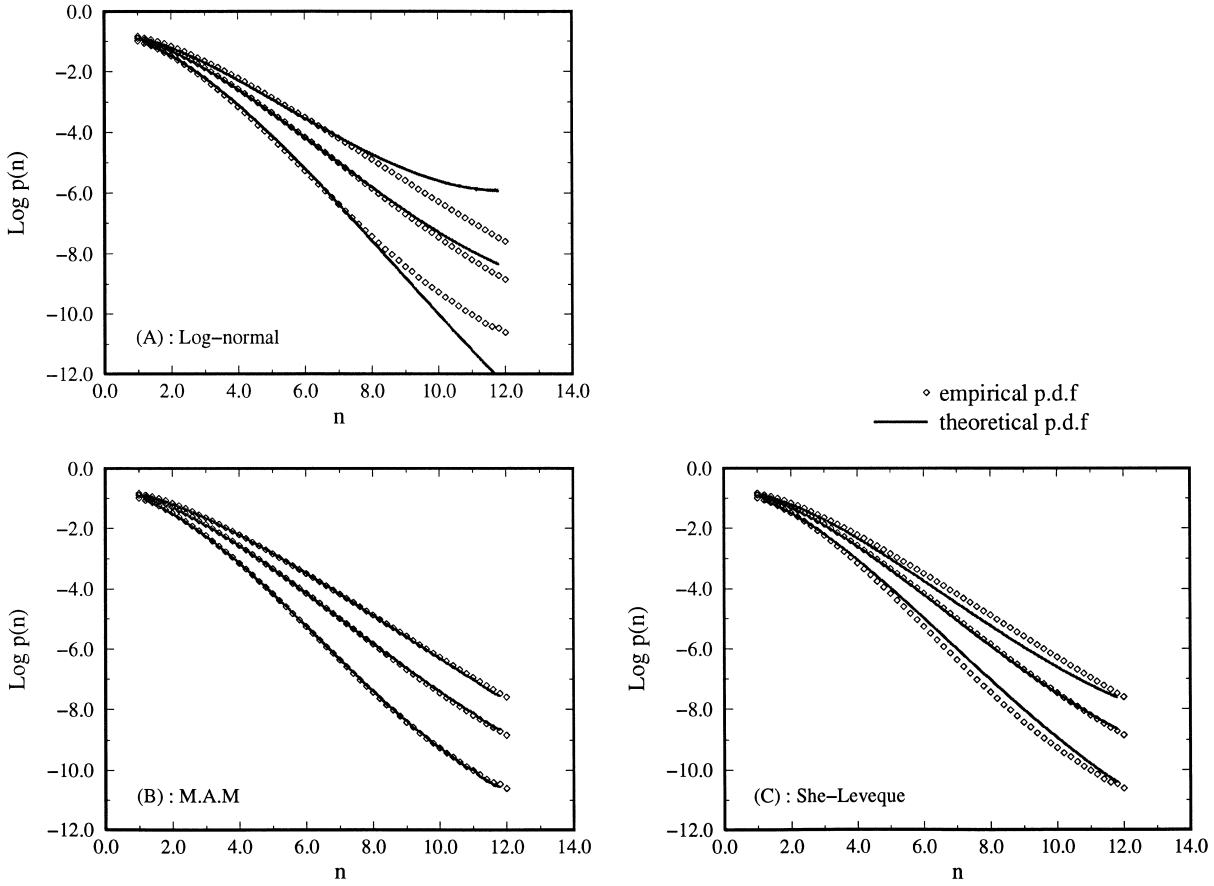


Fig. 10. Parametric plot of $\log p(n, \ell)$ for (A) log-normal model, (B) MAM model, (C) She-Lévêque model.

## Appendix A

### *A.1. Laplace's method*

Eq. (3) can be written in the form

$$S(n, \ell) = \int_{-\infty}^{+\infty} \exp\left\{\log\left(\frac{\ell}{\ell_G}\right)\left[n\frac{\mathcal{L}_u}{\log(\ell/\ell_G)} + \frac{\log p(\mathcal{L}_u, \ell)}{\log(\ell/\ell_G)}\right]\right\} \mathrm{d}\mathcal{L}_u \tag{A.1}$$

This integral has a critical point in $\mathcal{L}_u$, if $n$ obeys the relation

$$n(\mathcal{L}_u, \ell) = -\frac{\partial \log p(\mathcal{L}_u, \ell)}{\partial \mathcal{L}_u} \tag{A.2}$$

Taylor expanding the integrand around $n(\mathcal{L}_u, \ell)$ and performing the Gaussian integral yields

$$S(\mathcal{L}_u, \ell) = \left[-\frac{2\pi}{\partial^2 \log p(\mathcal{L}_u)/\partial \mathcal{L}_u^2}\right]^{1/2} \exp\left\{-\frac{\partial \log p(\mathcal{L}_u, \ell)}{\partial \mathcal{L}_u}\mathcal{L}_u + \log p(\mathcal{L}_u, \ell)\right\} + \mathcal{O}\left[\frac{1}{\log(\ell/\ell_G)}\right] \tag{A.3}$$

Eqs. (A.2) and (A.3), in logarithmic form, are the direct asymptotic formulae (20) and (21).

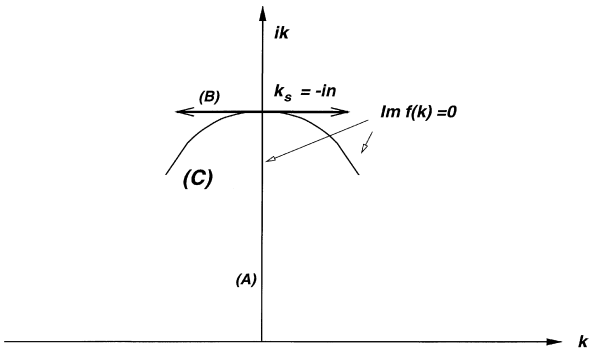


Fig. 11. Steepest descent method – Determination of integral curve (C).

*A.2. Steepest descent method*

The integral of Eq. (7) can be written in the form

$$p(\mathcal{L}_u) = \frac{1}{2\pi}\int_{-\infty}^{+\infty} \mathrm{e}^{\log(\ell/\ell_G) f(k)}\,\mathrm{d}k \tag{A.4}$$

with

$$f(k) = \frac{1}{\log(\ell/\ell_G)}[-\mathrm{i}k\mathcal{L}_u + \log S(\mathrm{i}k, \ell)] \tag{A.5}$$

The function $f(k)$ is real for $k = -\mathrm{i}n, n \in \mathbb{R}$. Consider $n_s$, such that

$$\left[\frac{\mathrm{d}f(k)}{\mathrm{d}k}\right]_{k=k_s=-\mathrm{i}n_s} = 0$$

thus

$$\mathcal{L}_u(n_s, \ell) = \frac{\partial \log S(n, \ell)}{\partial n} \tag{A.6}$$

then Taylor expanding $f$ around $k_s$, shows that $f$ is also real on a curve (C) parallel to the real axis and crossing the imaginary axis at $k_s$ (see Fig. 11 ).

The basic idea of the steepest descent method [19] is to make a deformation of the contour of integration of Eq. (A.4) from the real axis to (C). If such a deformation can be made, it follows that

$$p(\mathcal{L}_u, \ell) = (2\pi)^{-1}\int_{(C)} \mathrm{e}^{\log(\ell/\ell_G) f(k)}\,\mathrm{d}k \tag{A.7}$$

The steepest descent method, amounts to use the Laplace method on integral of Eq. (A.7). The main contribution of Eq. (A.7) is at the maximum of $f$ on (C), i.e. at the saddle point $k_s$ thus, it is enough to compute $f(k_s)$ and $f''(k_s)$. Using Eq. (A.5), we find

$$f(k_s) = \frac{1}{\log(\ell/\ell_G)}[-n\mathcal{L}_u + \log S(n, \ell)]$$

$$f'(k_s) = \frac{1}{\log(\ell/\ell_G)}\left[-\mathcal{L}_u + \frac{\partial \log S(n, \ell)}{\partial n}\right]\mathrm{i}$$

$$f''(k_s) = -\frac{1}{\log(\ell/\ell_G)}\frac{\partial^2 \log S(n,\ell)}{\partial n^2}$$

and thus, the value of Eq. (A.7) is given at leading order by

$$p(\mathcal{L}_u,\ell) = (2\pi)^{-1}\left[\frac{2\pi}{-\log(\ell/\ell_G)f''(k_s)}\right]^{1/2} \mathrm{e}^{\log(\ell/\ell_G)f(k_s)} + \mathcal{O}\left[\frac{1}{\log(\ell/\ell_G)}\right] \tag{A.8}$$

Eqs. (A.6) and (A.8) in logarithmic form are the inverse asymptotic formulae for Eqs. (16) and (17).

### A.3. Higher-order corrections

It is possible to compute higher order corrections to the asymptotic relations (A.3) and (A.8) but the calculation is rather lengthy. Note that Eqs. (A.2) and (A.6) are valid at all orders. The higher-order correction to Eq. (A.3) is explicitly given by (see [18] for a derivation)

$$\begin{aligned} S(\log u,\ell) = \exp\left[-\frac{\partial \log p(\log u,\ell)}{\partial \log u}\log u + \log p(\log u,\ell)\right]\sqrt{\frac{2\pi}{-\partial^2 \log p(\log u,\ell)/\partial \log u^2}} \\ \times\left\{1 - \frac{5\left\{\partial^3 \log p(\log u,\ell)/\partial \log u^3\right\}^2}{24\left\{\partial^2 \log p(\log u,\ell)/\partial \log u^2\right\}^3} + \frac{\partial^4 \log p(\log u,\ell)/\partial \log u^4}{8\left\{\partial^2 \log p(\log u,\ell)/\partial \log u^2\right\}^2} + \mathcal{O}\left[\frac{1}{\log(\ell/\ell_G)^2}\right]\right\} \end{aligned} \tag{A.9}$$

The correction to expression (A.8) is given by

$$\begin{aligned} p(n,\ell) = \exp\left[\log S(n,\ell) - n\frac{\partial \log S(n,\ell)}{\partial n}\right]\sqrt{\frac{1}{2\pi(\partial^2 \log S(n,\ell)/\partial n^2)}} \\ \times\left\{1 - \frac{5\left\{\partial^3 \log S(n,\ell)/\partial n^3\right\}^2}{24\left\{\partial^2 \log S(n,\ell)/\partial n^2\right\}^3} + \frac{\partial^4 \log S(n,\ell)/\partial n^4}{8\left\{\partial^2 \log S(n,\ell)/\partial n^2\right\}^2} + \mathcal{O}\left[\frac{1}{\log(\ell/\ell_G)^2}\right]\right\} \end{aligned} \tag{A.10}$$

It is very easy to check that the higher-order corrections term are of order $1/\log(\ell/\ell_G)$.

### A.4. Explicit computation of the errors in an integrable case

In the general case, where $\log S(n,\ell) = \log(1-n^2)\log(\ell/\ell_G)$, it is possible to explicitly integrate Eq. (7). The result is [24]

$$p(\log u,\ell) = \frac{\sqrt{2/\pi}[\log u]^{(-1/2-\log(\ell/\ell_G))}\mathcal{BK}(-1/2-\log(\ell/\ell_G),|\log u|)}{[1/2]^{\log(\ell/\ell_G)}\Gamma[-\log(\ell/\ell_G)]} \tag{A.11}$$

where $\mathcal{BK}(n,z)$ is the modified Bessel function of the second type, which is the solution to

$$z^2\frac{\mathrm{d}^2 y}{\mathrm{d}z^2} + z\frac{\mathrm{d}y}{\mathrm{d}z} - (z^2+n^2)y = 0$$

The asymptotic evaluation of Eq. (7) gives the following result

$$\log u(n,\ell) = -\log(\ell/\ell_G)\frac{2n}{1-n^2} \tag{A.12}$$

The probability density function is given at leading order by

$$\log p_1(n,\ell) = \log\left[\frac{\ell}{\ell_G}\right]\frac{2n^2}{1-n^2} + \log\left[\frac{\ell}{\ell_G}\right]\log(1-n^2) - \frac{1}{2}\log\left[-\log(\ell/\ell_G)\frac{4\pi(1+n^2)}{(-1+n^2)^2}\right]$$

and the probability density function including correction Eq. (A.10) is given by

$$\log p_2(n,\ell) = \log p_1(n,\ell) + \frac{1}{\log(\ell/\ell_G)}\frac{-9+27n^2-3n^4+n^6}{24(1+n^2)^3}$$

By defining

$$h(n,\ell) = \frac{\log u(n,\ell)}{\log(\ell/\ell_G)} = -\frac{2n}{1-n^2}$$

and

$$\mu_1(n,\ell) = \frac{\log p_1(n,\ell)}{\log(\ell/\ell_G)}$$

$$\mu_2(n,\ell) = \frac{\log p_2(n,\ell)}{\log(\ell/\ell_G)}$$

and defining the exact ratio $\mu_{\text{exact}}(n,\ell) = \log p(\log u,\ell)/\log(\ell/\ell_G)$ with $p(\log u,\ell)$ defined by Eq. (A.11) and $\log u$ by Eq. (A.12), we can study the behavior of the related errors as a function of $n$ and $\log\ell$

$$E_1(n,\ell) = \frac{\mu_1(n,\ell)-\mu_{\text{exact}}(n,\ell)}{\mu_{\text{exact}}(n,\ell)} \tag{A.13}$$

$$E_2(n,\ell) = \frac{\mu_2(n,\ell)-\mu_{\text{exact}}(n,\ell)}{\mu_{\text{exact}}(n,\ell)} \tag{A.14}$$

It can be seen in Fig. 12 that the errors vanish in the limit $n \to 1$ ($\log u \to \infty$) and, when $n$ is fixed, in the limit $\log(\ell/\ell_G) \to -\infty$. Furthermore, the convergence in $\log(\ell/\ell_G)$ shows that the higher order term has been correctly taken into account.

*A.4.1. Asymptotic relations in the $n \to \infty$ limit*

If the probability density function is Gaussian or exponential, it is possible to define asymptotic relations in the fixed $\ell$, $n \to \infty$ limit. Indeed, in the special case where

$$\log p(\mathcal{L}_u) = -\mathrm{e}^{\mathcal{L}_u} \tag{A.15}$$

we define

$$S(n) = \int_{-\infty}^{+\infty} \mathrm{e}^{n\mathcal{L}_u - \exp(\mathcal{L}_u)}\,\mathrm{d}\mathcal{L}_u \tag{A.16}$$

the critical point $n$ is given by $\log n = \mathcal{L}_u$, translating Eq. (A.16) at the critical point $\mathcal{L}_u = x + \log n$, we find

$$S(n) = n^n \int_{-\infty}^{+\infty} \mathrm{e}^{n[x-\exp(x)]}\,\mathrm{d}x$$

Using the direct method (A.3)

$$\log n(\mathcal{L}_u) = \mathcal{L}_u$$

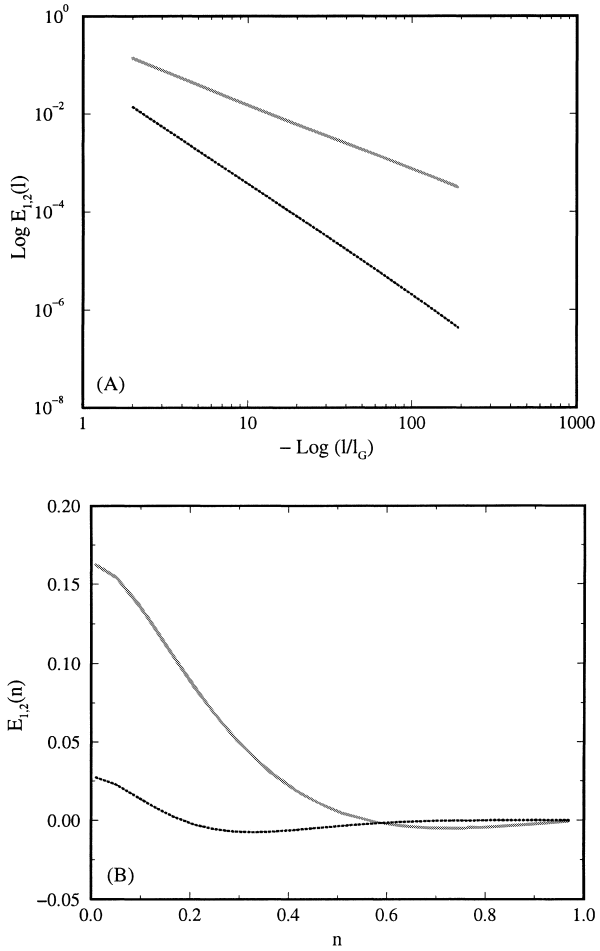


Fig. 12. Errors $E_1$ (A.13), $E_2$ (A.14) for $n = 0.1$ and $2 < \log(\ell/\ell_G) < 200$ (see (A)). Errors $E_1$ (A.13), $E_2$ (A.14) for $\log(\ell/\ell_G) = -2$ and $0 < n < 1$ (see (B)).

$$\log S(\mathcal{L}_u) = \mathrm{e}^{\mathcal{L}_u}(-1 + \mathcal{L}_u) + \frac{1}{2}\log\left[\frac{2\pi}{e^{\mathcal{L}_u}}\right] \tag{A.17}$$

which is equivalent to Stirling formulae. Note that the asymptotic relations in the $n \to \infty$ limit can be extended to Gaussian integrals. Setting $\mathrm{e}^{\mathcal{L}_u} = u$, Eq. (A.16) can be written as

$$S(n) = \int_{-\infty}^{+\infty} \mathrm{e}^{n\mathcal{L}_u - \exp(\mathcal{L}_u)}\,\mathrm{d}\mathcal{L}_u = \int_0^{+\infty} u^{n-1}\,\mathrm{e}^{-u}\,\mathrm{d}u \tag{A.18}$$

and thus $S(n) = \Gamma(n)$. Setting $u = y^2/(2\sigma^2)$, yields

$$S(n) = 2[2\sigma^2]^{-n}\int_0^{+\infty} \mathrm{e}^{-y^2/(2\sigma^2)} y^{2n-1}\,\mathrm{d}y \tag{A.19}$$

which shows that the moment of order $n' = 2n - 1$ of a Gaussian distribution can be asymptotically evaluated in the $n \to \infty$ limit by Eq. (A.17). It is thus possible to use the asymptotic relation in this way in the case of a Gaussian unifractal probability density function.

## References

[1] A.N. Kolmogorov, The local structure of turbulence in incompressible viscous fluid for very large Reynolds number, C. R. Acad. Sci., USSR 30 (1941) 9–13.
[2] A.N. Kolmogorov, On degeneration decay of isotropic turbulence in an incompressible viscous liquid, C. R. Acad. Sci., USSR 31 (1941) 538–540.
[3] A.N. Kolmogorov, Dissipation of energy in locally isotropic turbulence, C. R. Acad. Sci., USSR 32 (1941) 16–18.
[4] A.N. Kolmogorov, A refinement of previous hypotheses concerning the local structure of turbulence in a viscous incompressible fluid at high Reynolds number, J. Fluid Mech. 13 (1962) 82–85.
[5] A.M. Obukhov, Some specific features of atmospheric turbulence, J. Fluid Mech. 13 (1962) 77–81 .
[6] U. Frisch, Turbulence: The Legacy of A.N. Kolmogorov, Cambridge University Press, Cambridge, 1995.
[7] E.A. Novikov, R.W. Stewart, The intermittency of turbulence and the spectrum of energy dissipation, Izv. Akad. Nauk. SSSR Ser. Geoffiz. 3 (1964) 408–413.
[8] U. Frisch, P.L. Sulem, M. Nelkin, A simple dynamical model of intermittent fully developed turbulence, J. Fluid Mech. 87 (1978) 719–736.
[9] B.B. Mandelbrot, On intermittent free turbulence, in: Turbulence of Fluids and Plasmas, Brooklyn Polytechnic Institute, 1968.
[10] B.B. Mandelbrot, Intermittent turbulence in self-similar cascades: divergence of high moments and dimension of the carrier, J. Fluid Mech. 62 (1974) 331–358.
[11] C.W. Van Atta, W.Y. Chen, Structure functions of the turbulence in the atmospheric boundary layer over the ocean, J. Fluid Mech. 44 (1970) 145–159.
[12] F. Anselmet, Y. Gagne, E.J. Hopfinger, R.A. Antonia, High order velocity structure functions in turbulent shear flow, J. Fluid Mech. 140 (1984) 63–89.
[13] Y. Gagne, Etude Expérimentale de l'intermittence et des singularités dans le plan complexe en turbulence développée. PhD Thesis, Université de Grenoble, France, 1987.
[14] G. Parisi, U. Frisch, On the singularity structure of fully developed turbulence, in: M. Ghil, R. Benzi, G. Parisi (Eds.), Turbulence and Predictability in Geophysical Fluid Dynamics, Proc. Int. School of Physics 'E. Fermi', 1983, Varenna, Italy, North-Holland, Amsterdam, 1985, pp. 84–87.
[15] B.B. Mandelbrot, Random multifractal: negative dimensions and the resulting limitations of the thermodynamic formalism, Proc. R. Soc. London, Ser. A 434 (1991) 79–88.
[16] P. Kalilasnath, K.R. Sreenivasan, G. Stolovitsky, Probability density of velocity increments in turbulent flows, Phys. Rev. Lett. 68 (1992) 2766–2769.
[17] R. Benzi, S. Ciliberto, R. Tripiccione, C. Baudet, F. Massaioli, S. Succi, Extended self-similarity in turbulent flows, Phys. Rev. E 48 (1993) R29-R32.
[18] J.M. Tchéou, Analyse statistique multifractale en turbulence pleinement développée et application à la finance. PhD Thesis, Ecole Normale Supérieure de Cachan, France, 1997.
[19] C.M. Bender, S.A. Orszag, Advanced mathematical methods for scientists and engineers, in: International Series in Pure and Applied Mathematics, McGraw-Hill, New York, 1978.
[20] J. Maurer, P. Tabeling, G. Zocchi, Statistics of turbulence between two counter-rotating disks in low temperature helium gas, Europhys. Lett. 26 (1994) 31–36.
[21] P. Tabeling, G. Zocchi, F. Belin, J. Maurer, H. Willaime, Probability density functions, skewness and flatness in large Reynolds number turbulence, Phys. Rev. E 53 (1996) 1613–1621.
[22] F. Belin, P. Tabeling, H. Willaime, Exponents of the structure function in a helium experiment, Physica D 93 (1995) 52–63.
[23] J.M. Tchéou, M.E. Brachet, Multifractal scaling of probability density function: a tool for turbulent data analysis, J. Phys. B 6 (1996) 937–943.
[24] I.S. Gradshtein, I.M. Ryshik, Table of Integrals Series and Products. Academic Press, New York, 1994.